092-543

SYNERGISTIC EFFECTS AND DEFLAGRATION ANALYSIS IN COMPOSITE SOLID PROPELLANT COMBUSTION

W. C. Strahle
J. C. Handley

November 1, 1975

FINAL REPORT – RESEARCH SPONSORED BY
THE OFFICE OF NAVAL RESEARCH

ONR Contract No. N00014-75-C-0332

(6) Synergistic Effects and Deflagration Analysis in Composite Solid Propellant Combustion.

(10) W. C. Strahle
J. C. Handley

(11) 1 November 1975 (12) 44p.

(9) Final Report, Research Sponsored by
The Office of Naval Research

(15) ONR Contract No. N00014-75-C-0332

Approved for Public Release; Distribution Unlimited

ABSTRACT

Using four common catalysts the existence and magnitude of synergistic effects upon burn rate are studied with HTPB-AP composite solid propellants. The effect under study is one whereby at a fixed total catalyst loading the mixture of two catalysts would be more effective in burn rate augmentation than a single catalyst. At 2000 psia all possible combinations of catalysts showed synergistic effects but the effects are weak and within the reproducibility range of the experiments. Ferric oxide and iron blue showed synergistic effects only at 300 and 2000 psia over the pressure range 300-2000 psia.

Analysis of the effect of binder-oxidizer reactions upon the surface shape of a two-dimensional sandwich has shown that a) the faster are these reactions the more deeply will the sandwich obtain a V-shape and b) these reactions are generally fast enough to indeed affect the surface shape.

TABLE OF CONTENTS

INTRODUCTION

The current investigation represents a continuation of the work initiated at the Georgia Institute of Technology, which has been presented in References 1 and 2. In these investigations two-dimensional composite solid propellant sandwiches of polycrystalline ammonium perchlorate (AP) oxidizer and hydroxyl terminated polybutadine (HTPB) binder were used to investigate various modes of catalytic behavior. Four proven burn rate modifiers which behave as catalysts have been used throughout these ongoing investigations. They are Harshaw Catalyst Cu 0202 P, ferric oxide, iron blue and ferrocene.

During the first phase of this investigation[1] the catalysts were loaded into either the oxidizer or binder or restricted to the binder-oxidizer interface of two-dimensional sandwiches. Vertical sandwich burn rates and oxidizer normal regression rates were obtained using cinephotomacrography techniques. Details of the surface structure were obtained by using the scanning electron microscope to observe partially burned samples. It was determined that if one effective catalyst was added to the oxidizer and another to the binder, there was a net increase of burn rate over that of the sum of the independent actions of the catalysts. This combined effect was denoted as a positive synergistic effect on sample burn rate. The existence of this synergistic effect for the four catalysts was systematically investigated[2] using the two-dimensional sandwiches. The Harshaw catalyst Cu 0202 P - ferric oxide system, Fig. 1, and iron blue-ferric oxide system, Fig. 2, were found to exhibit a positive synergistic effect over the entire pressure range, 600 to 2000 psia and the maximum synergistic effect at 600 psia, respectively. The burn rate ratio on Figs. 1 and 2 is the ratio of the burn rate of the catalysed sample to the burn rate of a pure AP-HTPB sample.

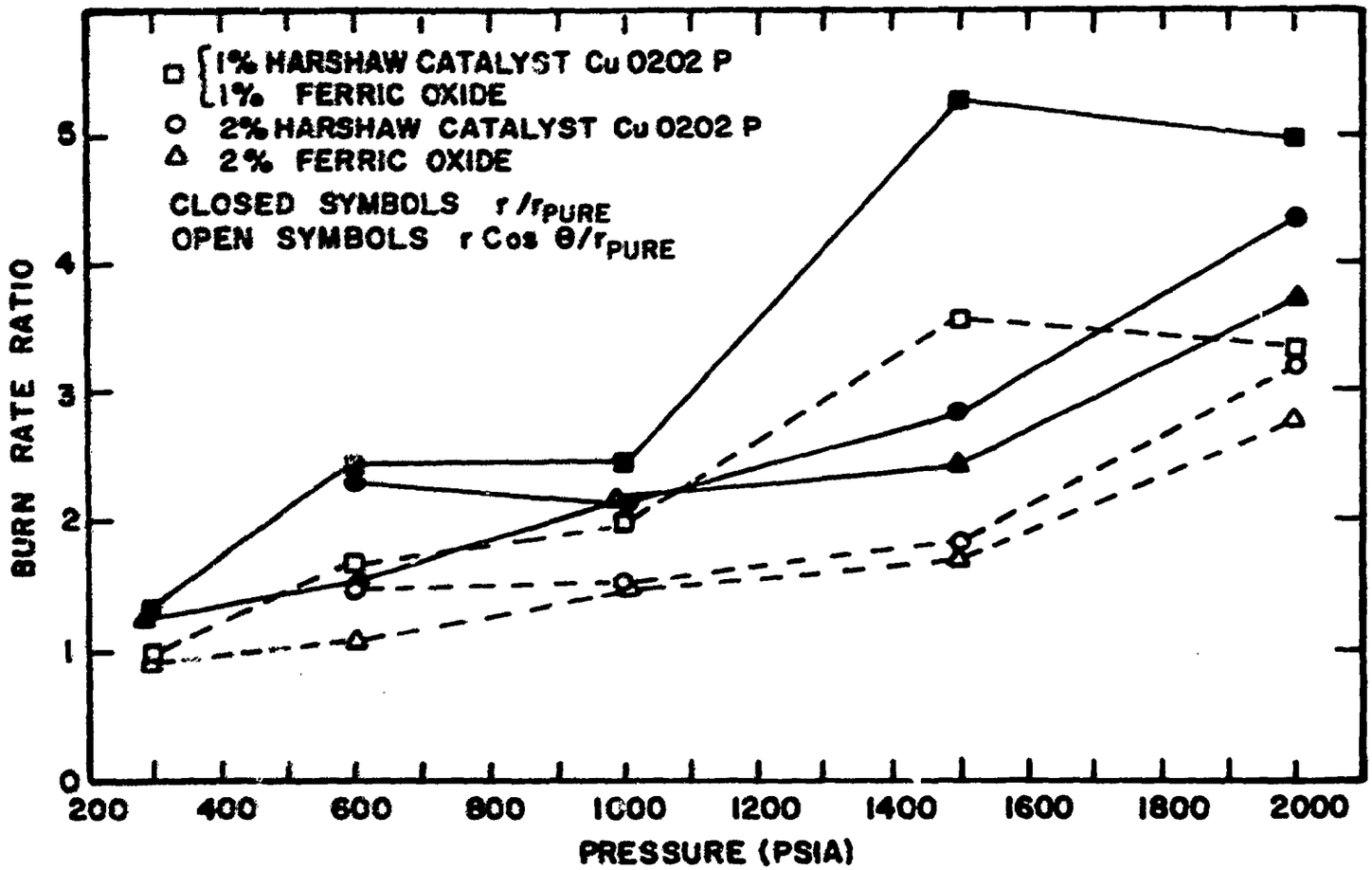

Figure 1. Synergistic Effect on Sandwich Vertical Burn Rate for Harshaw Catalyst Cu 0202 P and Ferric Oxide.

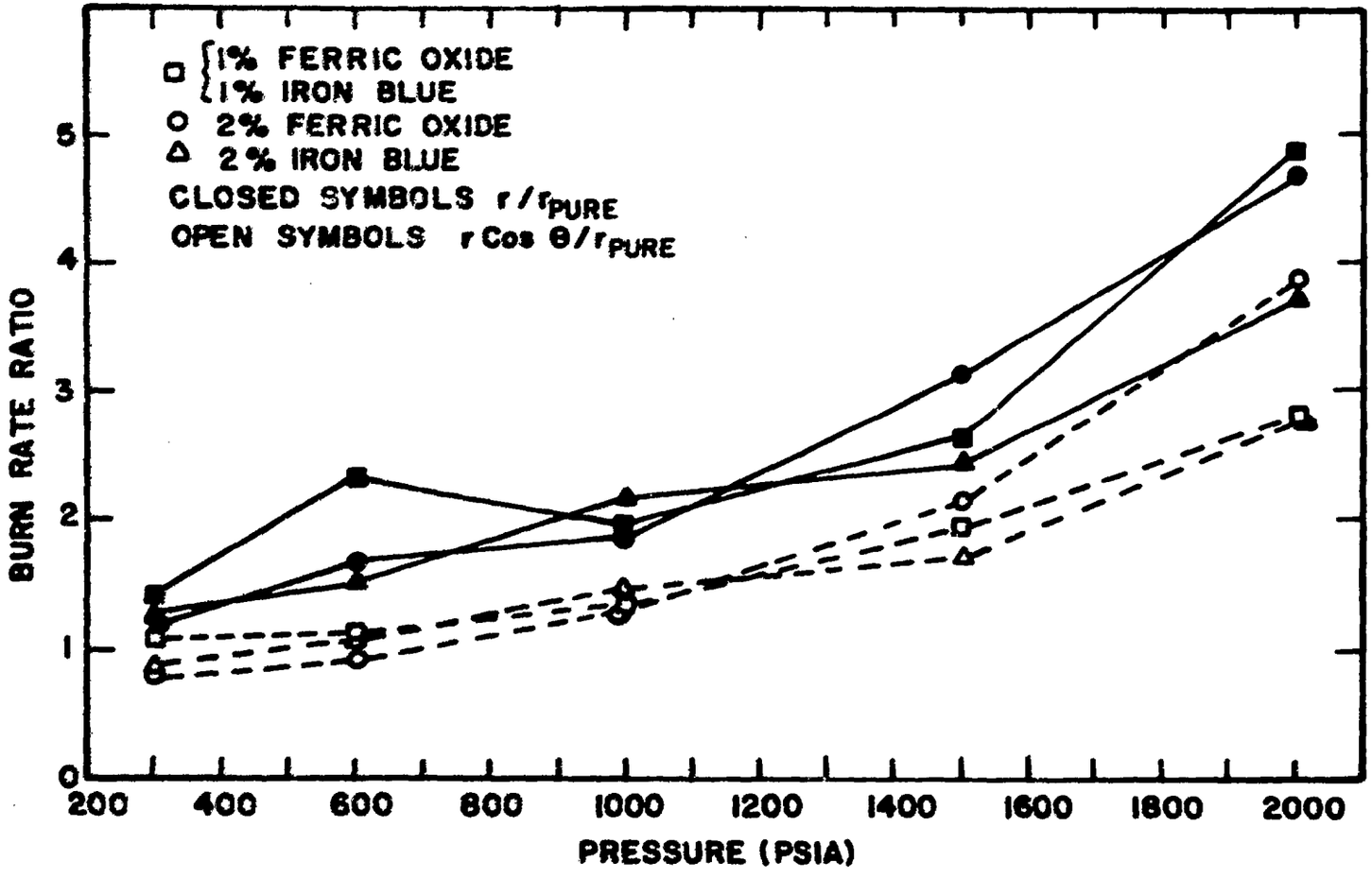

Figure 2. Synergistic Effect on Sandwich Vertical Burn Rate for Ferric Oxide and Iron Blue.

These two systems were chosen for further testing in cast propellant configurations. The initial samples were prepared with the same volumetric loading as in the sandwiches. The strands were prepared from a common lot of uncured composite propellant with an 82.7% solids to 17.3% binder loading. The oxidizer particle distribution was:

$$180\ \mu m < 70\% < 212\ \mu m$$

$$37\ \mu m < 30\% < 45\ \mu m\ .$$

The sample burn rate for the uncatalyzed propellant agreed with the data for propellant # 78 in the Princeton University test series [3]. The catalyst was added to the uncured propellant at a weight percent of 2.4%. Tests of the Harshaw catalyst Cu 0202 P - ferric oxide and iron blue-ferric oxide systems showed no positive synergistic effect at 600 psia[2].

These cast propellant samples were initially prepared to contain on average the same volumetric loading of catalyst as the sandwiches. But for the cast propellants all of the catalyst is suspended in the binder matrix, which constitutes 17w% of the sample. Since 2.4w% of catalyst was added to the cast propellant samples the binder matrix contained 14.2w% of the catalyst. The binder matrix for the sandwiches contained 4.4% of catalyst. This increase of catalyst in the binder affected the cure and the strength of the binder. This high catalyst loading in the binder may be above the amount required for maximum burn rate augmentation. In order to investigate this possibility further, a new set of samples were prepared using a reduced total catalyst loading of 1% catalyst by weight. This reduced the effective binder loading to 5.9%.

The current study has continued the investigation of synergistic effects on sample burn rate in cast composite propellants with 1w% of catalyst. An experimental procedure has been developed to produce a cast propellant that can be used as a con-

venient test vehicle for catalytic effects. An investigation of catalyst loading in the oxidizer of a cast propellant has been performed. Burn rates of these samples have been obtained at 600 and 2000 psia.

FUSE WIRE TESTS

Two separate batches of AP and HTPB were prepared for the initial tests of the addition of 1w% catalyst to the uncured propellant. The ratio of 82.7% solids (AP) to 17.3% binder (HTPB) was maintained, consistent with earlier tests[2]. The oxidizer particle distribution was maintained at

$$180\ \mu m < 70\% < 212\ \mu m$$

$$37\ \mu m < 30\% < 45\ \mu m\ .$$

Freon T F was mixed with the first batch of propellant. This decreased the viscosity of the mixture and allowed the propellant to be packed much easier in the teflon strand molds. The Freon T F could be removed by vaporization at room temperature or by vacuum in the curing oven. The samples were not sufficiently fluid to fill the voids as the freon vaporized. This yielded porous cast propellants. All of the oxidizer particles were premixed before the binder and catalyst were added to the second batch of propellant. This propellant was very difficult to mix and pack in the teflon molds. These samples resembled the first batch of samples. They were porous with a grainy appearance.

Thirteen fuse wire tests were conducted using samples from these two batches of propellants. Several variations of sample preparations were used. Different modes of inhibition were tried on the sides of the samples. Coatings of PVC, vaccum grease and epoxy were used along with water leaching of surface AP and increased flushing nitrogen flows. The results for all samples were the same. All fuse wires appeared to break simultaneously. Both batches of propellant

behaved similarly. This had not been encountered with the 2.41w% catalytic samples of Reference 2. There had been fluctuations of burn rates but not consistently high burn rates as indicated by these samples.

High speed motion pictures were taken of four samples from these two batches. Based on a frame rate of 1600 frames per second, the pure AP-HTPB sample and the 1% Harshaw catalyst Cu 0202 P sample exploded and burned in .015 seconds (24 frames). The 1% ferric oxide sample was completely consumed in .009 seconds (14 frames). The 1% ferric oxide-iron blue sample lasted for .022 seconds (36 frames).

It is believed that during manufacturing too narrow an AP particle size distribution was being employed, preventing binder wetting and good packing. It was decided to broaden the particle size distribution. Based on the length of time that was necessary to prepare fuse wire samples and the possible areas of uncertainty when the sample burns rapidly, it was decided to return to the cinephotomacrography for determination of sample burn rate and uniformity of burn rate. Poor quality propellant samples can be determined immediately from viewing the motion pictures.

CINEPHOTOMACROGRAPHY

The samples for these tests were prepared from common lots of uncured propellant. The solids to binder ratio was maintained at 82.7% to 17.3%. The bimodal AP particle distribution was broadened to:

$$\left.\begin{array}{l} 180\ \mu m < 35\% < 212\ \mu m \\ 125\ \mu m < 35\% < 180\ \mu m \end{array}\right\} 125\ \mu m < 70\% < 212\ \mu m$$

$$\left.\begin{array}{l} 45\ \mu m < 10\% < 63\ \mu m \\ 37\ \mu m < 10\% < 45\ \mu m \\ 10\% < 37\ \mu m \end{array}\right\} 30\% < 63\ \mu m$$

The oxidizer particle size distribution was prepared from ultra-pure ammonium perchlorate supplied by the Naval Weapons Center at China Lake, Calif. It was ground in a 0.3 gallon porcelain mill jar with an assortment of 1.3 and 2.5 cm ($\frac{1}{2}$" and 1") diameter balls. A series of seven 20.3 cm (8") diameter U.S.A. standard sieves was used to separate the ground AP. A motor driven sieve shaker was used to vibrate the sieves. The ground and sieved AP was stored in a sealed container and dried for 24 hours at 70° C before mixing with the binder.

The propellant was prepared by mixing all of the ingredients of the hydroxyl terminated polybutadiene with approximately one half of the largest size AP particles. This was mixed throughly and all of the AP particles are wetted with binder. This process was repeated with all AP particle sizes adding the finest AP last. This propellant was then divided for catalyst addition. A minimum of 10 grams of propellant was needed for each catalyzed sample. The proper amount of catalyst was added to the propellant and the mixing process repeated. This propellant was cast in 22 mm by 22 mm embedding molds and cured for seven days at 60°C.

The physical properties and appearance of the cured propellant was improved by the increased mixing time of the propellant and the broadened AP particle distribution. All of the oxidizer appeared to be wetted with binder. The cured propellant was cut into convenient sizes (7 mm x 6mm x 19mm) for testing in the high pressure combustion apparatus designed by Varney [4] and Jones [5].

These samples were similar in size to the two-dimensional sandwiches tested previously. This allowed the same cinephotomacrographic techniques to be used to observe the burning samples. The same nitrogen flows that were determined experi-

mentally for the sandwiches were used for smoke control. The latent image magnification was reduced to slightly less than 1:1 (image: actual). The motion picture speed was maintained at 1600 frames per second. The sample was oriented on the sample holder to allow observation of two sides of the sample. This indicated the uniformity of the burn and any effect of the light source on burn rate.

The sample burn rates and their uniformity were determined by recording sample profiles at 100 frame intervals by tracing the projected burning surface. These could be used to determine a burn rate every .0625 seconds.

The same combination of catalysts, Harshaw catalyst Cu 0202 P - ferric oxide and iron blue - ferric oxide, that were found to exhibit positive synergistic effects on sandwich vertical burn rate, were tested at 1w% addition to cast propellants. These two combinations of catalyst were determined by the two-dimensional screening experiment and were tested at 2.41w% catalyst addition at 600 psia[2].

Initially the six samples were tested at 600 psia. No positibe synergism was indicated, so a second set of samples were tested at 2000 psia. The results of both of these tests are shown in Table I.

TABLE I

Burn Rates for Cast Composite Propellant (11-22-74)

Catalyst	Burn Rate (in/sec) 600 psia			2000 psi		
	r	r/r_{pure}		r	r/r_{pure}	
None	.34	1		.66	1	
Harshaw Catalyst Cu 0202 P (CC)	.51	1.50		.74	1.12	
Ferric Oxide (IO)	.45	1.32	possible synergism	.83	1.26	possible synergism
Iron Blue (IB)	.54	1.59		.78	1.18	
CC & IO	.48	1.41	No	.80	1.21	Yes
IO & IB	.54	1.59	Yes	.88	1.33	Yes

A "positive" synergistic effect on sample burn rate is obtained when the burn rate of the sample with two effective catalysts present exceeds the burn rates of both of the corresponding samples with only one catalyst present. The total catalyst loading is maintained constant for all three samples. A "possible" synergistic effect on sample burn rate is obtained when the burn rate of the sample with two catalysts present is greater than the average of the burn rates for the two samples with only one catalyst present. Consequently, a "positive" synergism is also a "possible" synergism. A "negative" synergistic effect on sample burn rate is obtained when the burn rate of the sample with two catalysts present is less than the burn rates of both of the corresponding samples with only one catalyst present.

The Harshaw catalyst Cu 0202 P - ferric oxide system did not exhibit a positive synergism at either pressure, but there was a possible synergism indicated at 2000 psi. There was a positive synergistic effect on sample burn rate for the ferric oxide - iron blue system at 2000 psi. Because of this the ferric oxide - iron blue samples and their companion samples were tested over the pressure range 300 to 2000 psia. The results are shown in Figure 3. There was a positive synergistic effect at 300 and 2000 psia, a possible synergistic effect at 600 psia, and a negative effect at 1000 and 1500 psia. The positive synergistic effect on sample burn rate at 300 and 2000 psia along with a review of the favorable catalytic effect of ferrocene when it was restrained to the binder-oxidizer interface [1] led to a new evaluation of possible synergistic effects for all combinations of catalysts. Five new catalyst configurations were prepared to complete the test matrix. This included a sample with 1% ferrocene added, three samples with ½% of ferrocene and ½% of the other three catalysts and finally a ½% Harshaw catalyst Cu 0202 P and ½% iron blue sample. The results are shown in Table II for 2000 psia.

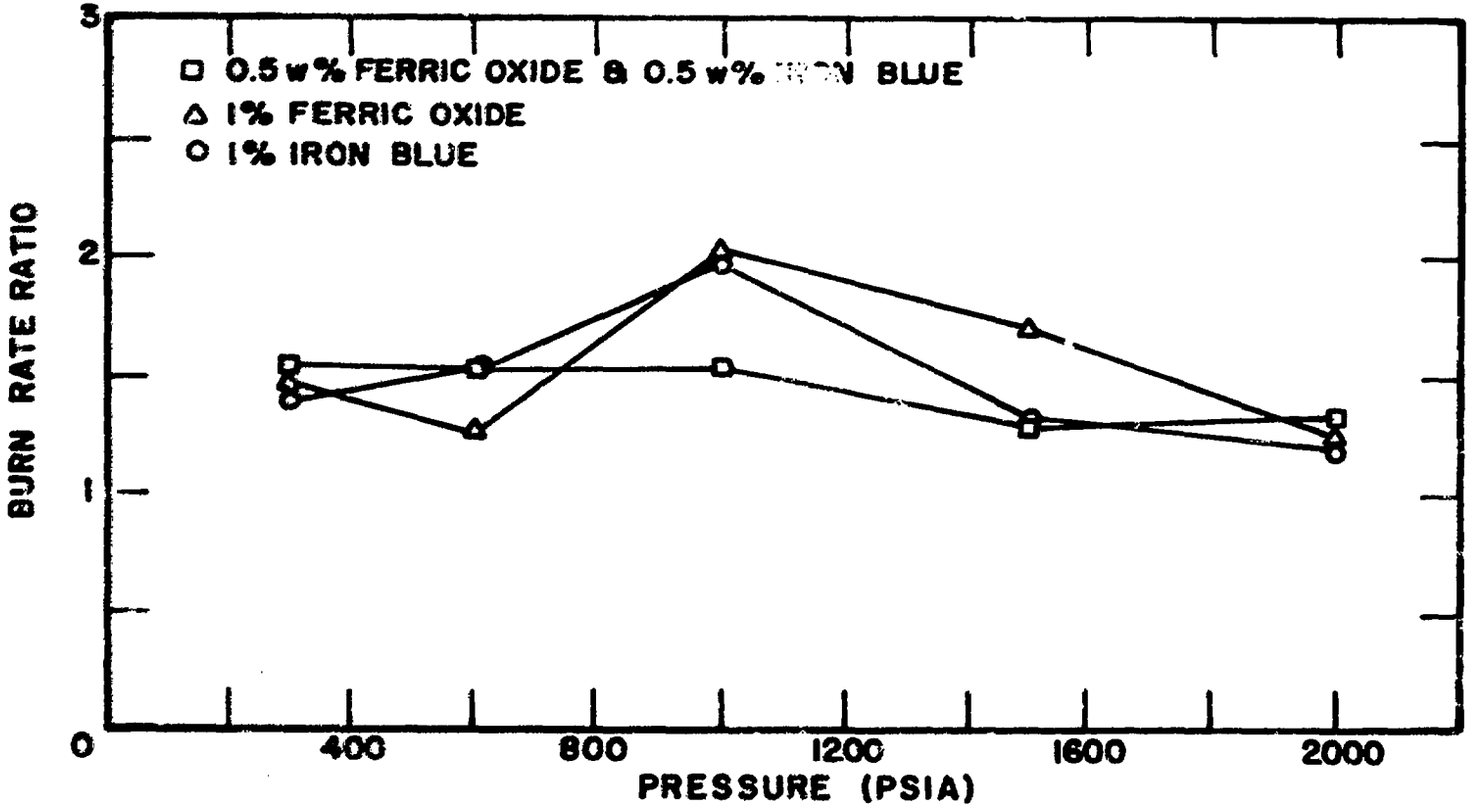

Figure 3. Synergistic Effect for Ferric Oxide-Iron Blue in Cast Composite Propellants.

TABLE II

Burn Rates for Cast Composite Propellant (5-8-75)

Catalyst	2000 psi Burn Rate (in/sec)	r/r_{pure}
None	.80	1
Ferrocene (F)	.75	.94
CC & IB	1.13	1.41
CC & F	.95	1.19
IO & F	.89	1.11
IB & F	.87	1.09

Initially these burn rates were ratioed with the pure cast propellant burn rate of Table I (11-22-74). These burn rate ratios are shown in the first column of Table III. A positive synergistic effect on sample burn rate was indicated for all new catalyst combinations. This meant that only the Harshaw catalyst Cu 0202 P - ferric oxide system did not yield a positive synergistic effect at 2000 psi. Six separate determinations of sample burn rate yielded a different average burn rate of the pure cast composite propellant (5-8-75). When this new burn rate, r_{pure} = .80 in/sec was used to ratio the burn rates of samples prepared from the propellant (5-8-75), the second column of burn rate ratios was obtained in Table III. The initial indication of five positive synergisms was reduced to positive synergisms for three systems.

Due to the apparent large difference of burn rate for the pure cast composite propellant samples a third batch of propellant was prepared. All combinations of the four catalysts and their comparison samples were prepared. The burn rates and their ratios are shown in Table IV for 2000 psia. There was a positive synergistic effect indicated for the iron blue - ferrocene system. All indications of synergistic effects were different from the other two batches of propellant. There

TABLE III

Burn Rate Ratios for Cast Composite

Propellants (11-22-74) and (5-8-75)
at 2000 psia

Catalyst	r/r_{pure} r_{pure} = .66 in/sec		r/r_{pure} r_{pure} = .66 in/sec or .80 in/sec	
None	1		1	
Harshaw Catalyst Cu 0202P(CC)	1.12		1.12	
Ferric Oxide (IO)	1.26		1.26	
Iron Blue (IB)	1.18		1.18	
Ferrocene (F)	1.14	Possible Synergism	.94	Possible Synergism
CC & IO	1.21	Yes	1.21	Yes
CC & IB	1.71	Yes	1.41	Yes
CC & F	1.44	Yes	1.19	Yes
IO & IB	1.33	Yes	1.33	Yes
IO & F	1.35	Yes	1.11	Yes
IB & F	1.32	Yes	1.09	Yes

appears to be a spread of up to .26 in/sec in the burn rate of the pure cast samples. This variation is as large as the burn rate augmentation obtained for most of the catalyzed samples both with single and double catalysts present. It is concluded that reproductibility with these small mixes prevents a conclusive demonstration of synergistic effects.

TABLE IV

Burn Rates for Cast Composite

Propellant (8-20-75)

Catalyst	r (in/sec)	r/r_{pure}	
None	.56	1	
Harshaw Catalyst Cu 0202 P (CC)	.78	1.39	
Ferric Oxide (IO)	.85	1.52	
Iron Blue (IB)	.78	1.39	
Ferrocene (F)	.65	1.16	
			Possible Synergism
CC & IO	.77	1.38	No
CC & IB	.78	1.39	?
CC & F	.62	1.11	No
IO & IB	.81	1.45	No
IO & F	.67	1.20	No
IB & F	.92	1.64	Yes

CATALYST LOADED INTO AP

Harshaw catalyst Cu 0202 P was selected for tests of loading in the oxidizer polycrystalline structure because of its catalysis of the AP deflagration process[1].

The oxidizer particles for the investigation of catalyst loaded into the oxidizer were prepared from special polycrystalline oxidizer disks. Ultra-pure ammonium perchlorate less than 37 μm in diameter was mixed with 1w% of catalyst and placed in the mold assembly designed by Varney [4]. Approximately 5 grams of this fine oxidizer mixture was pressed at one time. The polycrystalline disk was subjected to 30,500 psia for one hour. These disks were reground by hand in a motar and pestle and then sieved. All oxidizer particles less than 37 μm in diameter were discarded. 10% of all remaining sizes was retained for a catalyst loading determination. The remaining oxidizer with catalyst was cast into a solid propellant. The oxidizer particle distribution was:

125 μm < 43.7% < 212 μm

63 μm < 50.8% < 125 μm

37 μm < 5.5% < 63 μm

Comparison samples of pure AP-HTPB and 1w% of catalyst added to the AP-HTPB mixture were prepared with the same oxidizer particle distribution.

These three samples were tested at 600 and 2000 psia. The results are shown in Table V.

TABLE V

Harshaw Catalyst Cu 0202 P Loaded in AP

	Burn Rate (in/sec)	
Propellant	600 psia	2000 psia
Pure AP-HTPB	.45	.82
1% CC in AP-Pure HTPB	.54	.86
1% CC in HTPB-Pure AP	.69	1.44

The maximum burn rate was obtained for the catalyst added to the AP-HTPB mixture. This is essentially a binder-loaded cast composite propellant.

All three of the special distribution propellants were difficult to mix. The cured propellants were grainy and crumbly in sections. Two separate batches of the pure propellant were prepared and the burn rate varied as .82 ± .05 in/sec.

A procedure for determing the amount of catalyst remaining in the polycrystalline oxidizer structure was developed. The oxidizer mixture was placed in a 60 ml vacuum funnel with a built-in 40 mm diameter ultra-fine fritted glass filter disk. The ammonium perchlorate was dissolved by repeated washings with distilled water. The washing was continued for three cycles after the liquid showed no perchlorate ions when tested with a methylene blue indicator solution. This solution turns from dark blue to violet in the presence of the perchlorate ions. The material remaining in the filter was dried and weighed. A catalyst determination of the 10% of all size distributions used in the propellant was performed along with the oxidizer with a diameter less than 37 μm. This allowed a catalyst balance to be performed.

Initially 1w% of Harshaw catalyst was added to the AP. The measurement indicated a loading of 1.6 ± .3% by weight in the AP which went into the propellant. A catalyst balance was made by determining the amount of catalyst in the sieved polycrystalline oxidizer less than 37 μm in diameter. This balance indicated a possible oxidizer loading of .7 ± .2% by weight. The difference between these two indicated loadings is unresolved.

ANALYSIS

The work of Ref. (2) was extended to include the effect of binder-oxidizer reactions on the surface shape attained by a two-dimensional sandwich, assuming there are no melt flows. The work is presented in Appendix A. It is shown that,

indeed, fast binder-oxidizer reactions will force a sandwich to go to a V-shaped structure, as has been suspected from experimental observation and physical reasoning. More importantly, it appears that the oxidizer-binder kinetics are fast enough to influence the sandwich shape at usual deflagration pressures and that the AP flame is not the only heat source which influences the shape attained by the sandwich.

CONCLUSIONS

1. Although plagued by reproducibility problems, all possible combinations of the four catalysts investigated exhibited positive or possible synergistic effects on sample burn rate at a pressure of 2000 psia.
2. The synergistic effects are weak and within the range of the reproducibility of the experiments. Consequently, they are of doubtful practical utility with the catalysts investigated in these experiments.
3. The ferric oxide-iron blue system, which was the only system tested over the 300-2000 psia pressure range, exhibited weak posititive synergistic effects only at 300 and 2000 psia.
4. The cast propellant samples with Harshaw catalyst Cu 0202 P loaded in the oxidizer particles did not burn as fast as the binder loaded samples at 600 and 2000 psia. However, difficulties in the experimental determination of the actual catalyst loading in the oxidizer particles render the results inconclusive.
5. Analysis has shown that the faster are the binder-oxidizer reactions the more V-shaped will be a sandwich when deflagrating, reinforcing prior interpretation of sandwich shapes and the effect of catalysis of binder-oxidizer reactions on surface shape.

REFERENCES

1. Strahle, W. C., Handley, J. C. and Kumar, N., "Catalytic Behavior in Solid Propellant Combustion," Annual Summary Report for ONR Contract No. N0014-67-A-0159-0016, Georgia Institute of Technology, Atlanta, Georgia.

2. Strahle, W.C. and Handley, J.C., "Synergistic and Novel Effects in Composite Solid Propellant Combustion," Second Annual Summary Report for ONR Contract No. N0014-67-A-0159-0016, Georgia Institute of Technology, Atlanta, Georgia.

3. Steinz, J. A., Stang, P. L. and Summerfield, M., "The Burning Mechanism of Ammonium Perchlorate-Based Composite Solid Propellants," AMS Report No. 830 ONR Contract Nonr 1858 (32), February, 1969.

4. Varney, A. M., "An Experimental Investigation of the Burning Mechanisms of Ammonium Perchlorate Composite Solid Propellants," Ph. D. Dissertation, Georgia Institute of Technology, 1970.

5. Jones, H. E., "An Experimental Investigation Relating to the Combustion Mechanisms of Ammonium Perchlorate Composite Propellants," Ph.D. Dissertation, Georgia Institute of Technology, 1971.

APPENDIX A

Solid Propellant Sandwich Deflagration Analysis with Binder - Oxidizer Reactions

NOMENCLATURE

A	constants in the perturbation solution
c	distance above solid surface at which the mass fraction of $HClO_4$ vanishes
c_s	specific heat of solid phase
c_p	specific heat at constant pressure
C	deviation of c from the one-dimensional value
E	activation energy
g	dimensionless temperature, T/T_o
G	deviation of g from the one-dimensional value
h	specific enthalpy
$\hat{h}_o$	dimensionless specific enthalpy of formation h_o/c_pT_o
k	specific reaction rate constant
$\tilde{k}$	$k\rho^2/W^2$
$\hat{k}$	dimensionless preexponential factor
ℓ	linear transport operator
m	root for exponential solutions
$\dot{m}$	mass flow rate per unit area
q	endothermic heat of gasification
q_R	heat of reaction in the gas phase for the pure AP deflagration
r	burn rate
T	temperature
w	production rate, mass/volume/time
$\hat{w}$	dimensionless production rate
W	molecular weight
x	horizontal coordinate
y	vertical coordinate
Y	mass fraction
$\bar{Y}_{s_F}$	mass fraction of NH_3 at solid surface for one dimensional case

Y'	deviation of y_s' from one dimensional value
y	deviation of Y from $\bar{Y}$
F	$(1 + y_s'^2)^{1/2}$
α	thermal diffusivity or constants in perturbation solution
β	constants in perturbation solution
ε	dimensionless activation energy, E/RT_o
η	$y - y_s$
λ	thermal conductivity
ξ	$c_p \lambda_s / c_s \lambda_g$
ρ	density
τ_r	reaction time

Subscripts

o	cold solid values
1	reaction 1 or values at $\eta = c$
2	reaction 2
3	reaction 3
4	reaction 4
B	binder
F_1	NH_3
F_2	$HClO_4$
P_1	products of AP deflagration
P_2	products of reaction 2
P_3	products of binder-oxidizer reaction
AP	pertaining to one dimensional AP deflagration
g	gas phase
s	solid phase or at the solid-gas interface
s^+	in the gas phase at the solid-gas interface

Superscripts

*	dimensional quantity
'	differentiation with respect to x
-	pertaining to one-dimensional deflagration

INTRODUCTION

In Ref. (A-1) an analysis was conducted of the deflagration of a semi-infinite slab of ammonium perchlorate (AP) adjacent to a semi-infinite slab of binder. It was assumed that the binder was dry and passive so that reactions between the oxidizer and binder were too slow to be effective in driving the deflagration, and there were no melt flows to complicate the binder-oxidizer interface region. The slow reaction assumption required that the AP self-deflagration was the only mechanism responsible for pyrolysing the binder. Accordingly, the analysis could only be valid above the low pressure deflagration limit of the AP. In the current work the assumption of slow binder-oxidizer reactions is relaxed. However, for analytical tractability the no-melt-flow assumption is retained.

It was found in the previous treatment that regardless of binder type the AP would deflagrate with a nearly horizontal surface, far from the binder, and the surface would dip down slightly as the binder was approached. There was then a slope discontinuity at the binder-oxidizer interface and the binder, for usual binder properties, would assume a nearly vertical slope. By relaxation of the zero binder-oxidizer reaction rate assumption it is desired to find a modification to the surface slope that is invariably produced when a catalyst is added experimentally (A-2). That is, the AP assumes a small acute angle with respect to the nearly vertical binder. The reactions between the oxidizer and binder drive the interface region at a faster vertical burn rate than was possible when the AP deflagration above was responsible for the overall sandwich burn rate.

ANALYSIS

Reactions Considered

The simplest possible set of gas phase reactions which it appears possible to choose and still show the dominant processes is a set of reactions consistent

with Ref. (A-3). This is

$$
\begin{aligned}
F_1 + F_2 &\xrightarrow{k_1} P_1 \\
F_2 + B &\xrightarrow{k_2} P_2 \\
B + P_1 &\xrightarrow{k_3} P_3 \\
P_2 + F_1 &\xrightarrow{k_4} P_3
\end{aligned}
\qquad (1)
$$

Here F_1 denotes NH_3 and F_2 denotes $HClO_4$ presumed to be the major reactive products liberated from the AP surface. Species B is the binder pyrolysis product and P_1 is some product intermediate. P_3 is the final product of the oxidizer binder reaction. It is to be noted, of course, that these are a simplistic set of global reactions only chosen to describe gross effects.

In order to apply fundamental chemical kinetics to the above reactions it will first be assumed that F_1, F_2 and B have identical molecular weight W. Then P_1 has molecular weight 2W, as does P_2, and P_3 has molecular weight 3W. Using fundamental kinetics laws [A-4], the production rates of the various species may be written

$$
\begin{aligned}
w^* &= -\tilde{k}_1^* Y_{F_1} Y_{F_2} - \tfrac{1}{2} \tilde{k}_4^* Y_{P_2} Y_{F_1} \\
w_{P_2} &= \tilde{k}_1^* Y_{F_1} Y_{F_2} - k_2^* Y_{F_2} Y_B \\
w_B^* &= \tilde{k}_2^* Y_{F_2} Y_B - \tfrac{1}{2} \tilde{k}_3^* Y_B Y_{P_1} \\
w_{P_1}^* &= 2\tilde{k}_1^* Y_{F_1} Y_{F_2} - \tilde{k}_3^* Y_B Y_{P_1} \\
w_{P_2}^* &= 2\tilde{k}_2^* Y_{F_2} Y_B - \tilde{k}_4^* Y_{P_2} Y_{F_1} \\
w_{P_3}^* &= \tilde{k}_3^* Y_B Y_{P_1} + \tfrac{3}{2} \tilde{k}_4^* Y_{P_2} Y_{F_1}
\end{aligned}
\qquad (2)
$$

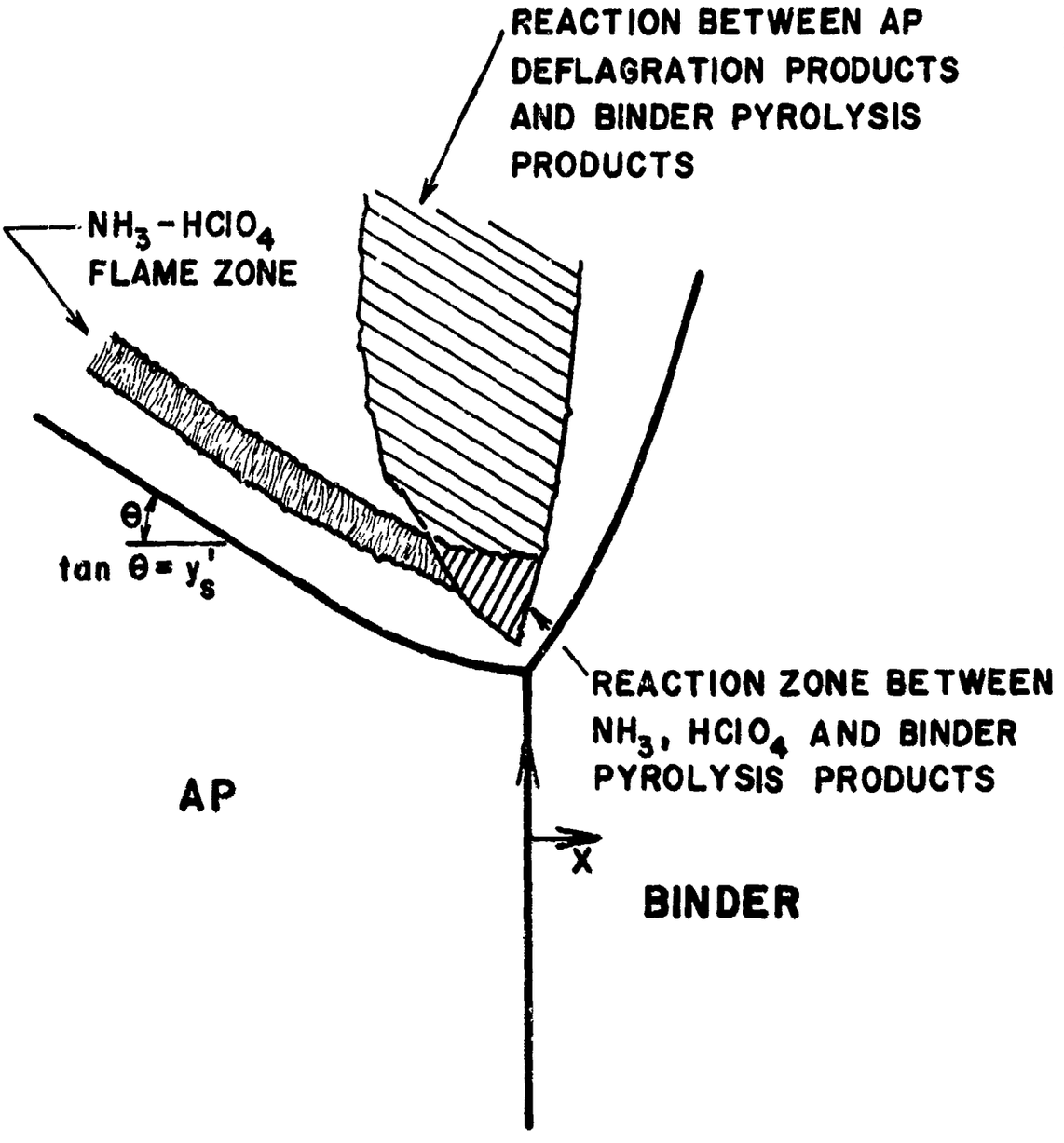

Figure A-1. Sandwich Deflagration Schematic.

These expressions must be used later in the species conservation equations. Substantial simplification will occur, however, if the boundary conditions on the species are first examined.

Species Boundary Condition

Making distance dimensionless by α_s^*/r^* and using Fick's law of diffusion, as in Ref. (A-1), the boundary condition at the gas-solid interface for any species may be written as

$$\left.\frac{\partial Y_i}{\partial n}\right)_{s^+} = \frac{\xi}{z}\left(Y_{i_s} - \frac{\dot{m}_{i_{s^+}}^*}{\dot{m}_{s^+}^*}\right) \tag{3}$$

where $\partial/\partial n = (1/z)(\partial/\partial y) - (y_s'/z)(\partial/\partial x)$. See Fig. (A-1) for the configuration. In order to evaluate the derivatives along the surface the same approach as used in Ref. (A-1) will be used. A functional form for Y_i is chosen as

$$Y_i = Y_{i_s} + (Y_{i_1} - Y_{i_s})(y - y_s)/c \tag{4}$$

with Y_{i_s}, Y_{i_1}, y_s, and c as unknowns to be determined from the conservation equations. All of these unknowns are functions of x. Note, however, because of the definition of c, $Y_{F_{2_1}} = 0$. Eq. (4) will allow evaluation of the derivative in Eq. (3). First, however, look at the mass flow ratio in Eq. (3). On the binder surface only binder can penetrate so the mass flow ratio is unity if i=B and is zero for all other species. On the AP surface, consistent with Ref. (A-5), P_1, F_1 and F_2 are the species for which the surface is a source. Let G be the fraction of the surface mass flow which is P_1 and then (1-G)/2 will be the mass flow ratio of F_1 and F_2. This "dilution coefficient", G, will be assumed independent of x, in accord with the independence on surface temperature shown in Ref. (A-5). Eq. (3) calculated for F_1 as an example yields

$$\frac{-Y_{F_{1_s}}}{c} - \frac{y_s'}{z}\left[Y_{F_{i_s}}'\right] = \frac{\xi}{z}\left[Y_{F_{1_s}} - \left(\frac{1-G}{2}\right)\right] \tag{5}$$

On the other hand, when evaluating Eq. (3) for F_1 on the binder but just at the

interface, more care must be taken. For no mass sources or sinks the Y_{i_l} and Y_{i_s} of Eq. (4) must be continuous at $x = 0$ and their first derivative must be continuous. However y_s' undergoes a discontinuity at $x = 0$. Therefore, Eq. (3) just to the right of the interface is

$$-\frac{1}{z_B}\,\frac{Y_{F_{l_s}}}{c}-\frac{y_{s_B}'}{z_B}\left[Y_{F_{l_s}}'+\frac{y_s'}{c}\,Y_{F_{l_s}}\right]=\frac{\xi}{z_B}\,Y_{F_{l_s}} \tag{6}$$

where it is understood that Eq. (6) is only good at $x = 0$. Eq. (5) is a boundary condition that applies all along $-\infty \le x \le 0$. The boundary condition on B is

$$\frac{1}{z}\,\frac{Y_{B_l}-Y_{B_s}}{c}-\frac{y_s'}{z}\left[Y_{B_s}'-y_s'\left(\frac{Y_{B_l}-Y_{B_s}}{c}\right)\right]=\frac{\xi}{z}\,Y_{B_s} \tag{7}$$

but right at $x = 0$

$$\frac{1}{z_B}\,\frac{Y_{B_l}-Y_{B_s}}{c}-\frac{y_{s_B}'}{z_B}\left[Y_{B_s}'-\frac{y_s'}{c}\,(Y_{B_l}-Y_{B_s})\right]=\frac{\xi}{z_B}\,(Y_{B_s}-1) \tag{8}$$

Eqs. (6) and (8) may now be investigated concerning orders of magnitude. A perturbation solution will be sought so that at $x = 0$, which is the binder-oxidizer interface, only a small perturbation on a one-dimensional AP deflagration will be taking place. That is, the P_2, P_3 and B mass fractions will be small compared with unity and the deviations of F_1, F_2 and P_1 mass fractions from their one-dimensional deflagration values will be small compared with unity. Guided by Ref. (A-1) it will be assumed that y_{s_B}' is large compared with unity and y_s' is small but that this product may be of order unity. Derivates in x will be of order ξ compared with unity and ξ is large. It is assumed that y_{s_B}' is of the order of ξ or larger and all perturbation quantities are of the order of $1/\xi$. From Ref. (A-1), c is of order $1/\xi$. Using these orders of magnitude in Eq. (8), the largest terms, which are of order ξ, are

$$y_{s_B}'\,Y_{B_s}'(0)=\xi \tag{9}$$

Splitting $Y_{F_{l_s}}$ and c into unperturbed and perturbed parts and using Eq. (6),

the boundary condition is

$$y'_{s_B} \; y'_{F_{1_s}}(0) = -\frac{\bar{Y}_{F_s}}{\bar{c}} \left(1 + y'_s \, y'_{s_B} \right) - \xi \bar{Y}_{F_s} \tag{10}$$

An equation similar to Eq. (10) holds for F_2. For P_1 the equation is

$$y'_{s_B} \; y'_{p_{1_s}}(0) = \frac{2\bar{Y}_{F_s}}{\bar{c}} \left(1 + y'_s \, y'_{s_B} \right) - \xi \left(1 - 2 \bar{Y}_{F_s} \right) \tag{11}$$

However, investigation of the interface conditions for P_2 and P_3 yield

$$Y'_{p_{2_s}}(0) = 0 = Y'_{p_{3_s}}(0) \tag{12}$$

Equations (9) - (12) hold at $x = 0$. The corresponding boundary conditions which hold for the unperturbed and perturbed quantities along the AP surface, $-\infty \leq x \leq 0$, are

$$\left(\xi + \frac{1}{\bar{c}} \right) \bar{Y}_{F_s} = \frac{\xi (1 - G)}{2} \tag{13}$$

for the unperturbed quantity and

$$\begin{aligned}
C \left(\bar{Y}_{F_s} / \bar{c}^2 \right) + \left(\xi + 1/\bar{c} \right) y_{F_{1_s}} &= 0 \\
C \left(\bar{Y}_{F_s} / \bar{c}^2 \right) + \left(\xi + 1/\bar{c} \right) y_{F_{2_s}} &= 0 \\
\left(\xi + 1/\bar{c} \right) y_{B_s} - y_{B_1} / \bar{c} &= 0 \\
\left(\xi + 1/\bar{c} \right) y_{p_{2_s}} - y_{p_{2_1}} / \bar{c} &= 0 \\
C \left(\bar{Y}_{p_{1_s}} - 1 \right) / \bar{c}^2 - \left(\xi + 1/\bar{c} \right) y_{p_{1_s}} + y_{p_{1_1}} / \bar{c} &= 0
\end{aligned} \tag{14}$$

for the perturbed quantities. In the above, terms of order $1/\xi$ compared to unity have been dropped.

Gas Phase Solution

The conservation equations have been developed in Ref. (A-1), so they will only be stated here. Using the variables $\eta \equiv y - y_s$, x instead of y, x, the

energy equation is

$$\ell\,(g) = \sum_{i=1}^{6} \hat{w}_i\, \hat{h}_{i_o}$$

$$\ell \equiv \frac{\partial^2}{\partial x^2} + z^2\, \frac{\partial^2}{\partial \eta^2} - 2\, y_s'\, \frac{\partial^2}{\partial \eta \partial x} - y_s''\, \frac{\partial}{\partial \eta} - \xi\, \frac{\partial}{\partial \eta} \qquad (15)$$

For species i the conservation equation is

$$\ell\,(Y_i) = \hat{w}_i \equiv - w_i^*\, \alpha^*\, c_p^* \,/\, (r^* \lambda_g^*) \qquad (16)$$

Combination of Eqs. (15) and (16) yields a simple homogeneous equation

$$\ell \left(g + \sum_{i=1}^{6} \hat{h}_{i_o}\, Y_i \right) = 0 \qquad (17)$$

In Eq. (15) the operator ℓ contains $z^2 = 1 + y_s'^{\,2}$. To the accuracy of the analysis $y_s'^{\,2}$ may be neglected compared to unity. For the unperturbed deflagration of AP, field quantities are functions of η alone. The solution for the AP deflagration has been presented in Ref. (A-1), except for the modification due to the dilition coefficient which is included in this work. The solution is

$$\overline{Y}_{F_{1_s}} \left(\frac{1}{\bar{c}} + \xi \right) = \xi \left(\frac{1-G}{2} \right) = Q$$

$$Q \equiv \hat{k}_1\, Y_{F_{1_s}}^2\, \bar{c} \int_o^1 \left(1 - \frac{\eta}{\bar{c}}\right)^2 \exp\left\{ - \varepsilon_1 \,/\, \left[\bar{g}_s + (\bar{g}_1 - \bar{g}_s)\, \frac{\eta}{\bar{c}} \right] \right\} d\left(\frac{\eta}{\bar{c}}\right)$$

$$\bar{g}_1 - \bar{g}_s = 2\, q_R\, \overline{Y}_{F_{1_s}}$$

$$q_R \equiv \hat{h}_{F_{1_o}} - \hat{h}_{p_{1_o}} \qquad (18)$$

In this work the thermodynamic properties of F_1 and F_2 are assumed identical to each other, for simplicity. All numerical computations have been performed for $\xi = 9.0$, $\bar{g}_1 = 4.022$, $\bar{g}_s = 2.93$, $G = .75$, $\bar{c} = .119$ and $\overline{Y}_{F_{1_s}} = .0634$. This corresponds to burning at 800psia, but the dimensionless results are quite insensitive to

pressure, as explained in Ref. (A-1).

The solution of Eqs. (14) and (15) is by an integral technique. Using Eq. (4) as a guessed form for the mass fractions and $g - g_s = (g_1 - g_s)\ \eta/c$ for the temperature profile, Eqs. (16) and (17) are integrated in η from 0 to c. This yields ordinary differential equations in x. However, appearing in these equations from integration of the second term in ℓ from Eq. (15) is the η - derivative of the appropriate quantity evaluated at $\eta = c$. This is an unknown. To eliminate this unknown, as discussed in Ref. (A-1), the parabolic form of Eqs. (14) and (15) are used at $\eta = c$. That is, in Eqs. (14).

$$\frac{\partial^2 Y_i}{\partial x^2}\Big)_{\eta=c} - \xi \frac{\partial Y_i}{\partial \eta}\Big)_{\eta=c} = -\hat{w}_{i_{\eta=c}}$$

is used to eliminate $\partial Y_i/\partial\eta)_{\eta=c}$ in favor of the x - derivative and reaction rate. A similar operation holds for Eq. (17).

The next step in the solution is to let each unknown be represented by its unperturbed, one-dimensional value plus a perturbation component. The equations are then split into unperturbed equations and perturbation equations and the perturbation equations are then linearized. The unperturbed equations have Eqs. (18) as the solution, after using Eq. (13).

It is first instructive to view the solution for the binder mass fraction. The differential equation is

$$\begin{aligned} &y''_{B_s}\ (\bar{c}/2) + y''_{B_1}\ (\bar{c}/2 + 1/\xi) \\ &\quad + (y_{B_s} - y_{B_1})(\xi + 1/\bar{c}) = \hat{k}_2 \left\{ y_{B_s} I_{2_s} + y_{B_1} I_{2_1} \right\} \\ &\quad + \tfrac{1}{2} \hat{k}_3 \left\{ y_{B_s} I_{3_s} + y_{B_1} I_{3_1} \right\} + \tfrac{1}{2} \hat{k}_3 y_{B_1} e^{-\mathcal{E}_3/\bar{g}_1} \end{aligned} \qquad (19)$$

where the reaction rate integrals are evaluated from the unperturbed solution

$$I_{2_s} = \int_0^{\bar{c}} \bar{Y}_{F_s} \left(1 - \eta/\bar{c}\right)\left(1 - \eta/\bar{c}\right) e^{-\mathcal{E}_2/g} \, d\eta$$

$$I_{2_1} = \int_0^{\bar{c}} \bar{Y}_{F_s} \left(1 - \eta/\bar{c}\right) e^{-\mathcal{E}_2/g} \, d\eta$$

$$I_{3_s} = \int_0^{\bar{c}} \bar{Y}_{p_1}(\eta) \left(1 - \eta/\bar{c}\right) e^{-\mathcal{E}_3/g} \, d\eta$$

$$I_{3_1} = \int_0^{\bar{c}} \bar{Y}_{p_1} e^{-\mathcal{E}_3/g} \, d\eta$$

Notice that all I's are positive. Now viewing the binder boundary condition in Eqs. (14), $y_{B_s} \propto y_{B_1}$. Consequently, Eq. (19) is a homogeneous, linear second order differential equation with the solution

$$y_{B_s} = A_{B_s} e^{m_B x}$$

Making the required substitution m_B satisfies

$$m_B^2 = \frac{\left(\xi + 1/\bar{c}\right)\left(\xi + \gamma\right) + \mathcal{E}/\bar{c}}{\left(\xi + 1/\bar{c}\right)\left(\bar{c}/2 + 1/\xi\right) + 1/2} \tag{20}$$

where

$$\mathcal{E} = \hat{k}_2 I_{2_s} + \frac{1}{2}\hat{k}_3 I_{3_s}$$

$$\gamma = \hat{k}_2 I_{2_1} + \frac{1}{2}\hat{k}_3 I_{3_1} + \frac{1}{2}\hat{k}_3 e^{-\mathcal{E}_3/\bar{g}_1}$$

By inspection, therefore, m_B^2 is positive and m_B has two real, equal roots of opposite signs. The positive sign is accepted so that y_B will decay to zero at $x \to -\infty$. The constant of integration, A_{B_s} is determined by application of Eq. (9)

$$A_{B_s} = \xi/(m_B y'_{s_B})$$

The binder solution is therefore completed without knowledge of the behavior of the other mass fractions. Either reaction 2 or reaction 3 will increase m_B [see Eq. (20)] as the reaction rates increase. This has the effect of lowering

the amount of binder present in the gas phase [Eq. (21)] and of increasing the decay rate of binder as x proceeds away from zero. These are obvious physical facts since reactions 2 and 3 are disappearance reactions for the binder gases. Also note from Eq. (20) that m_B is indeed order ξ, if $\mathcal{E}$ is less than or equal to order unity. As a consequence y'_B is of the order of ξy_B, as asserted above. For $\mathcal{E} = \gamma = 0$, $m = 6.73$. Note furthermore that m_B is independent of $\bar{y}'_s$, under the restriction already imposed that $\bar{y}'_s$ is of order $1/\xi$.

All other mass fractions do not behave in an autonomous manner, however. The differential equation derived from continuity of the P_2 species, for example, yields

$$y''_{p_{2_s}} (\bar{c}/2) + y''_{p_{2_1}} (\bar{c}/2 + 1 \xi)$$

$$+ (y_{p_{2_s}} - y_{p_{2_1}})(\xi + 1/\bar{c}) = - 2 \hat{k}_2 \left\{ y_{B_s} I_{2_s} + y_{B_1} I_{2_1} \right\}$$

$$+ \hat{k}_4 \left\{ y_{p_{2_s}} I_{4_s} + y_{p_{2_1}} I_{4_1} \right\} \qquad (22)$$

where, as before,

$$I_{i_s} = \int_o^{\bar{c}} \bar{Y}_F (\eta)(1 - \eta/\bar{c}) \, e^{-\mathcal{E}_i/\bar{g}} \, d\eta$$

$$I_{i_1} = \int_o^{\bar{c}} \bar{Y}_F (\eta) \, e^{-\mathcal{E}_i/\bar{g}} \, d\eta$$

Considering that $y_{p_{2_s}} \propto y_{p_{2_1}}$ from Eqs. (14), Eq. (22) is a linear, second order equation in, say, P_{2_s}, but it is inhomogeneous because of the appearance of the binder mass fractions. It follows, therefore that $y_{p_{2_s}}$ will have a solution of the form

$$y_{p_{2_s}} = A_{p_{2_s}} e^{m_{p_2} x} + \alpha_{p_{2_s}} e^{m_B x}$$

It may be verified by substitution that the root to the homogeneous equation, m_{p_2}, increases with an increase in rate of the destruction reaction, reaction 4.

Application of Eq. (12) yields

$$A_{p_{2_s}} = -\alpha_{p_{2_s}} m_B/m_{p_2}$$

Continuing for P_3, the solution would look like

$$y_{p_{3_s}} = A_{p_{3_s}} e^{m_{p_3}} + \alpha_{p_{3_s}} e^{m_{p_2}x} + \beta_{p_{3_s}} e^{m_B x}$$

since the production of P_3 depends upon both B and P_2. However, since P_3 is never destroyed m_{p_3} is determined by Eq. (20), setting $\mathcal{E} = \gamma = 0$. Here $m_{p_3} = m = 6.73$ and all decay scales other than a fixed m are set by m_{p_2} and m_B.

The situation with F_1, F_2 amd P_1 are more complex, however, since they contain unperturbed as well as perturbed components. Only two of them need be considered, however, since

$$y_{F_1} + y_{F_2} + y_{p_1} + y_{p_2} + y_{p_3} = 0$$

Here y_{p_1} will be eliminated and only F_1 and F_2 are considered. Furthermore, consider now the case where k_2 and k_4 are zero (only a diffusion flame between the binder and AP deflagration products exists). In this case the equations for F_1 and F_2 are the same, as are the boundary conditions. Consequently $y_{F_1} = y_{F_2}$, as is obvious since there are no chemical reactions that prefer one over the other.

The differential equation for conservation of F_1 (or F_2) is

$$C''(\bar{Y}_{F_s}/2) + y''_{F_{1_s}}(\bar{c}/2) + y_{F_{1_s}}/\bar{c} - C\bar{Y}_{F_s}/\bar{c}^2$$

$$+ Y''\bar{Y}_{F_s} + \xi y_{F_{1_s}} = (\partial Q/\partial Y_{F_{1_s}}) y_{F_{1_s}} + (\partial Q/\partial c) C$$

$$+ (\partial Q/\partial y_1) G_1 + (\partial Q/\partial g_s) G_s \qquad (23)$$

where the derivatives of Q may be evaluated from Eq. (18). The unknowns are now $C, y_{F_{1_s}}, Y', G_1$ and G_s. The boundary condition of Eqs. (14) provides an algebraic

relation between C and $Y_{F_{1_s}}$, A second algebraic condition comes from the assumption of an equilibrium gas-solid interface (A-5, A-1), whereby

$$Y_{F_{1_s}} = \tilde{b}_F e^{-\mathcal{E}_B/g_s}, \quad y_{F_{1_s}} = \frac{G_s \mathcal{E}_B}{\bar{g}_s^2} \bar{Y}_{s_F} \tag{24}$$

A fourth equation in the five unknowns is obtained by integrating Eq. (15) and applying the perturbation procedure

$$\begin{aligned}(G_1'' + G_s'')(\bar{c}/2) + (G_s - G_1)(\xi + 1/\bar{c}) \\ + G_1''/\xi + \sum_{F_1,F_2,P_3,B} (\hat{h}_{i_o} - \hat{h}_{p_{1_o}})\{(y_{i_1}'' + y_{i_s}'')(\bar{c}/2) \\ + y_{i_1}''/\xi + (y_{i_s} - y_{i_1})(\xi + 1/\bar{c})\} = 0\end{aligned} \tag{25}$$

Equation (25) is not a homogeneous equation in the five unknowns because underneath the summation sign sit y_{p_s} and y_B, whose solutions are now known. In the current case the operation on P_3 in Eq. (25) is the homogeneous operator which wipes out the $e^{m_{p_3}x} = e^{mx}$ solutions. One is therefore left with only $e^{m_B x}$ type of behavior. The only way for the four equations in five unknowns to have a solution and still satisfy the boundary condition of Eq. (10) is to let

$$\begin{aligned} G_1 &= A_{g_1} e^{m_B x}, \quad C = A_c e^{m_B x} \\ Y' &= A_Y' e^{m_B x}, \quad G_s = A_{g_s} e^{m_B x} \\ Y_{F_{1_s}} &= Y_{F_{2_3}} = A_{Y_F} e^{m_B x} \end{aligned}$$

and use the boundary condition as an additional equation. It is to be noted that this procedure also holds if $\hat{k}_3 = 0$, the case of a purely inert binder. This latter case is the one treated by Ref. (A-1), but the solution there did not involve Eq. (9). It is now believed that Ref. (A-1) is in error since Eq. (9) must be satisfied for consistency. In any event, following the solution procedure, eliminating C and G_s and recalling that in Eq. (10) $y_s'(0) = \bar{y}_s' + A_y'$, there result three equations

in three unknowns of the form

$$A_{11}\, A_{g_1} + A_{12}\, A_{Y_F} = 3\, \gamma_{B_s}\, (\hat{h}_{p_{3_0}} - \hat{h}_{p_{1_0}}) \left[\varepsilon + (1 + c\, \xi)\, \gamma \right]$$

$$A_{21}\, A_{g_1} + A_{22}\, A_{Y_F} + A_{23}\, A_{Y'} = 0$$

$$A_{32}\, A_{Y_F} + A_{33}\, A_{Y'} = - \frac{\bar{Y}_{F_s} \left[\xi + (1 + \bar{y}_s'\, y_{s_B}')\, /\bar{c} \right]}{m_B\, y_{s_B}'} \qquad (26)$$

It may be verified in Eq. (26) that $A_{11} < 0$ and for excthermic reaction between B and P_1, the heat of formation difference in the first of Eq. (26) is negative. Since ε and γ are positive, the first of Eq. (26) clearly shows that the reaction tends to elevate g_1.

RESULTS

Consider first the solution for no reactions, $\varepsilon = \Gamma = 0$. For various y_{s_B}' and $\bar{y}_s'$ values the solutions to Eq. (26) are shown on Fig. A-2 as A_{g_1} vs $y_s'(0) = \bar{y}_s' + A_{Y'}$. The values for y_{s_B}' increase as one moves to the right along any curve of fixed $\bar{y}_s'$. It is seen first of all that there are no solutions for which $y_s'(0) > 0$. Furthermore, in regimes where $g_1 - \bar{g}_1$ are less than zero, which is the only physically reasonable regime, since the binder is a heat sink, $y_s' < \bar{y}_s'$. This means that the AP surface turns down to attempt to intersect the binder at an acute angle, rather than an obtuse angle. This is demanded by the gas phase solution alone and does not depend upon binder or AP properties in the solid phase. This character of the solution is somewhat counter to the author's intuition. It was expected that the AP would curve upward as the binder is approached.

For the case with reaction consider a high activation energy case so that γ is dominated by the last term and $\varepsilon << \gamma$. As an example take $\gamma = 0.15$ and

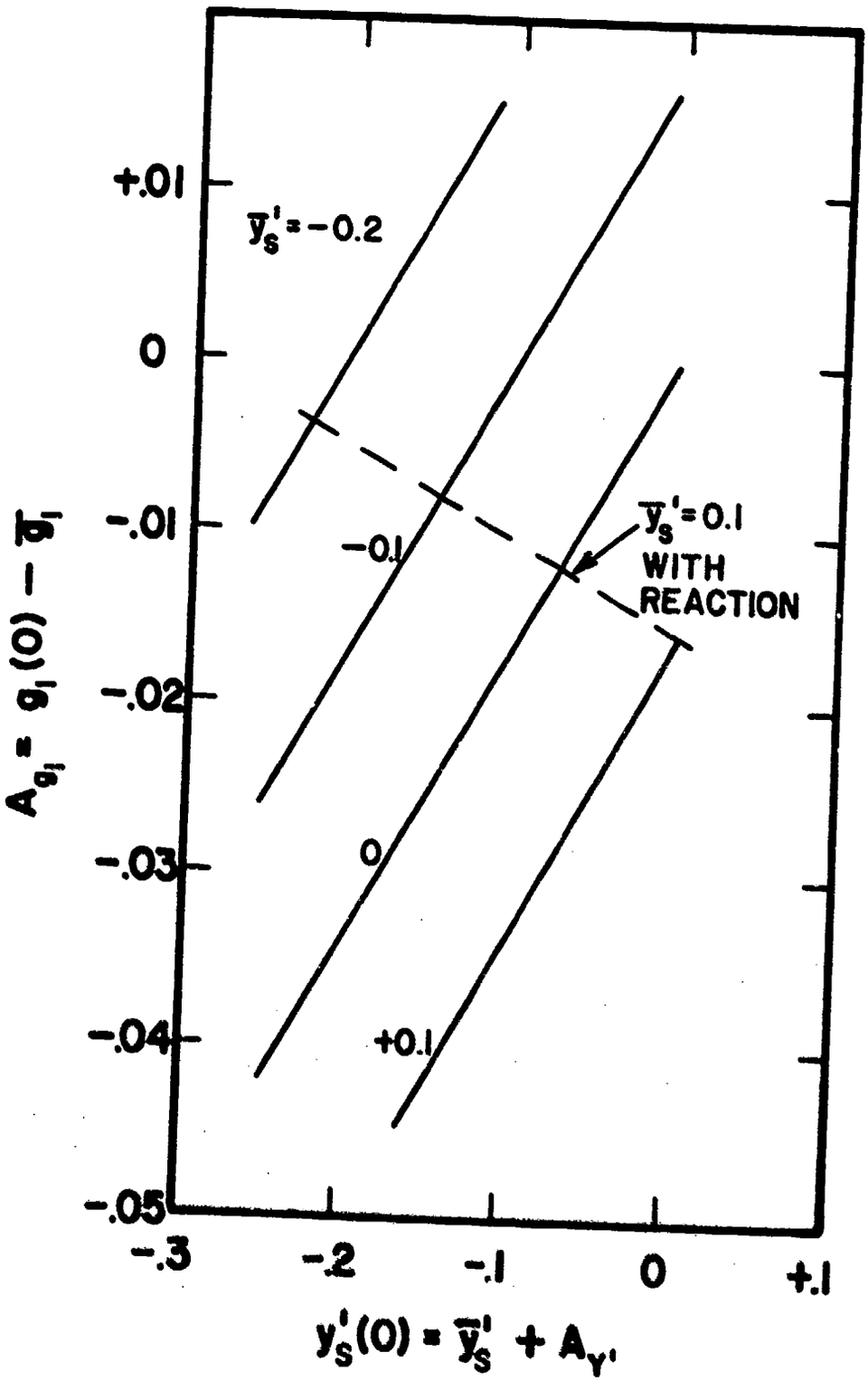

Figure A-2. Temperature at the Edge of the AP Flame as a Function of the Surface Slope at the Binder-Oxidizer Interface.

$\hat{h}_{p_{3_o}} - \hat{h}_{p_{1_o}} = -10$. On Fig. A-2 the dashed line shows the solution for $\bar{y}_s' = 0.1$. The temperature is, of course, elevated as compared with the no reaction case. Here there is no good physical argument to reject solutions for $A_{g_1} > 0$. However, only one solution curve is shown and for $\bar{y}_s' = 0.1$, $A_{g_1} < 0$.

In order to show which binder properties belong to each point on the curves of Fig. A-2 one must consider first the solution for the solid phase heat transfer. This solution was obtained in Ref. (A-1). By inspection of that solution, invoking the continuity of the heat transfer vectors in the solid and gas phases at the intersection of the binder and oxidizer, and applying the order of magnitude arguments, the solution for the binder heat of gasification is

$$q_B = m_B A_{g_s} y'_{s_B} + \left[1 + y'_{s_B} y'_s(0) \right] \left[\frac{\bar{g}_1 - \bar{g}_s}{\xi \bar{c}} + 1 - \bar{g}_s \right] \qquad (27)$$

It turns out, therefore, that the result is independent of the solid phase solution. This is a remarkable property of the problem. The final link to the binder is the pyrolysis law. As stated in Ref. (A-1) this is

$$\frac{1}{\left(1 + y'^{\,2}_{s_B} \right)} = \frac{b_B}{r} e^{-\mathcal{E}_B/\bar{g}_s} \qquad (28)$$

Given the activation energy, b_B is directly determined by y'_{s_B}, since $r = r_{A_p}$ consistent with the orders of magnitudes considered here. Then Eq. (27) determines the allowable q_B for any given $\bar{y}_s'$, which is the eigenvalue of the problem.

The results of this calculation are plotted for the no reaction case in Fig. A-3. Given a set of binder properties determines the eigenvalue y_s' on this plot. The disappointing result is that within the solution constraint that $\bar{y}_s'$ is small there are no solutions for binder properties of interest. Shown, for example, are the CTPB and HTPB points for properties taken from Ref. (A-6). There simply are no solutions to the problem for which $A_{g_1} < 0$ at large positive q_B. What

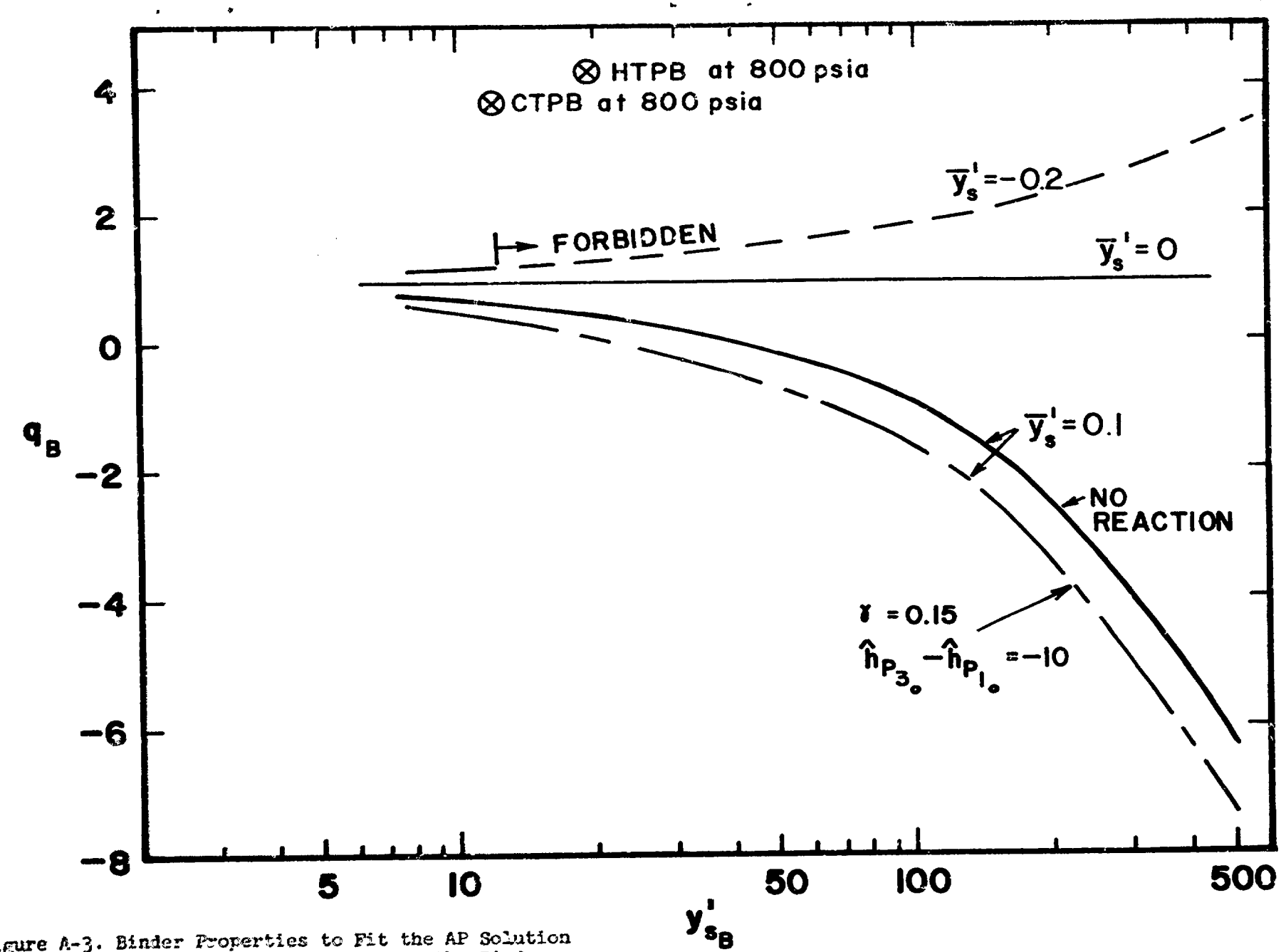

Figure A-3. Binder Properties to Fit the AP Solution with Surface Slope Far from the Binder as a Parameter; Reaction and No-Reaction Cases.

must occur for binders of interest is one must consider the fully nonlinear set of equations. Nevertheless, this solution may be used as a guide to investigate the qualitative effect of parameter changes.

Within the regime of allowable solutions, which basically limits the solution to small positive or negative q_B and $\bar{y}_s' > 0$, in increase in pyrolysis rate at fixed q_B increases $\bar{y}_s'$. An increase in heat of gasification at fixed pyrolysis rate (y_{s_B}' fixed) decreases the slope of the AP far from the interface ($\bar{y}_s'$ decreases).

For the case with reaction, considered above, the solution for $\bar{y}_s' = 0.1$ is shown on Fig. A-3. Exothermic reaction shifts all of the curves to lower q_B for fixed y_{s_B}'. Therefore, for a fixed set of binder properties the exothermic reactions decrease $\bar{y}_s'$. That is, the solution says that reactions tend to promote an acute angle between the oxidizer and binder, as is experimentally observed.

Tracing through the nondimensionalization procedure and for the numbers used here a characteristic reaction time is given by $1/\tau_r^* = k_3^* \; e^{-\mathcal{E}_3/\bar{g}_1} \; \gamma_{B_s} \; \rho^*/w^*$, and $\tau_r^* \approx 10^{-4}$ sec at 800 psia for $\gamma_{B_s} = 0.1$ (which depends on y_{s_B}' through Eq. (9). From Ref. (A-7) a typical reaction time under these conditions may be computed to be 10^{-5} sec. Therefore, typical reaction times are well within the range that a significant impact would be made on the sandwich shape by the binder-oxidizer reactions. Furthermore, for completeness reactions 2 and 4 should be considered. However, because of the limited applicability of this solution together with the qualitative information already gleaned from the solution, no further computations will be made.

CONCLUSIONS

1. A linearized solution using an integral technique has been found to the problem

of a deflagrating semi-infinite slab of AP adjacent to a semi-infinite slab of binder which is capable of reaction with the AP in the gas phase. The solution was found to only be valid for binders which are difficult to gasify (low pyrolysis rates) and with low or negative (exothermic) heats of gasification. A further restriction to the solution is that there are no melt flows.

2. For typical reaction times the binder-oxidizer reactions are fast enough to substantially affect the deflagration rate. The effect is to make the slab of AP intersect the binder at an acute angle, giving the appearance that the interface region is driving the deflagration rate, which it is.
3. The solution predicts that as one approaches the binder along the AP surface the AP surface becomes convex from above, which is somewhat counter to physical intuition.

REFERENCES

A-1. Strahle, W. C., "Solid Propellant Sandwich Deflagration Analysis," AIAA J., Vol. 13, May 1975, pp. 640-646.

A-2. Strahle, W. C., "Catalytic Effects in the Combustion of AP-HTPB Sandwiches to 3200 psia," Combustion Science and Technology, Vol. 8, Sept.-Dec., 1974, pp. 297-304.

A-3. Beckstead, M. W., Derr, R. L. and Price, C. F., "A Model of Composite Solid Propellant Combustion Based on Multiple Flames," AIAA J., Vol. 8, Dec. 1970, pp. 2200-2207

A-4. Williams, F. A., Combustion Theory, Addison-Wesley, Reading, 1965, p. 4.

A-5. Guirao, C. and Williams, F. A., "A Model for Ammonium Perchlorate Deflagration between 20 and 100 atm," AIAA J., Vol. 9, July 1971, pp. 1345-1356.

A-6. Cohen, N.S., Fleming, R. W. and Derr, R. L., "Role of Binder in Solid Propellant Combustion," AIAA Paper 72-1121, New Orleans, La. 1972.

A-7. Myers, B. F. and Bartle, E. R., "Reaction and Ignition Delay Times in the Oxidation of Propane," AIAA J., Vol. 7, Oct. 1969, pp. 1862-1869.